Journal of Renewable Materials

Tech Science Press

DOI: 10.32604/jrm.2024.053741

ARTICLE

Effect of Processing and Cultivar on Thermo-Chemical Properties of Australian-Grown Hemp Hurd (*Cannabis sativa* L.)

Johannes Fehrmann[1,*], Benoit Belleville[1], Barbara Ozarska[1], Maya Ismayati[2] and Wahyu Dwianto[2]

[1]School of Agriculture, Food and Ecosystem Sciences (SAFES), Faculty of Science, The University of Melbourne, Melbourne, 3121, Australia

[2]Research Center for Biomass and Bioproducts, National Research and Innovation Agency (BRIN), Jakarta, 16911, Indonesia

[*]Corresponding Author: Johannes Fehrmann. Email: jfehrmann@unimelb.edu.au

Received: 09 May 2024 Accepted: 19 June 2024 Published: 06 September 2024

ABSTRACT

This study explored the thermo-chemical properties of industrial hemp hurd with different provenances, maturity stages, and retting protocols. The findings were then compared to hemp hurd used in the fabrication of citric acid-bonded ultra-low-density hemp hurd particleboard. Pyrolysis-gas chromatography-mass spectrometry (Py-GC/MS), Fourier-transform infrared spectroscopy (FTIR), and thermogravimetric analysis (TGA) were employed to document the variability of the hurd and comprehend the potential impact on biobased composite applications. The choice of cultivar, maturity stage, and processing modality significantly influenced the chemical composition, presence of functional groups, and thermal stability of the hurd. Py-GC/MS revealed substantial variations in the lignin-to-carbohydrate (L/C) ratio, along with the absence of fatty acids in certain cultivars. While FTIR signals confirmed consistent functional groups, differences in peak intensities were indicative of carbohydrate variations associated with maturity and retting duration, impacting the availability of hydroxyl groups for, i.e., interparticle bonding in citric acid-based bio-composites. Furthermore, it was observed that shorter retting durations initially enhanced the thermal resistance, but prolonged retting led to accelerated degradation, significantly reducing the hurd's residual mass. The findings indicated notable differences among the samples, emphasizing the importance of investigating variables such as provenance/cultivar, maturity, and processing modality. This assessment is essential to ensure effective agronomic practices that align the raw material characteristics with the specific requirements of intended applications, such as the fabrication of biobased hemp hurd composites.

KEYWORDS

Hemp hurd; material characterization; chemical analysis; thermal analysis

1 Introduction

The decreasing availability of sustainable timber for wood-based panels (WBPs) motivates research into residual biomass from various horticultural and agricultural crops as alternative lignocellulosic raw materials. The by-products of many food crops are increasingly examined as substitutes or additives to traditional timber raw material in the development of innovative bio-composites. Crop residues offer the advantage of local abundance and short growth cycles with much attention recently given to industrial hemp

(*Cannabis sativa* L.). The renewed global interest in hemp cultivation typically arises from the plant's exceptional environmental credentials [1,2], carbon sink potential [3] and versatile array of consumables and products [4], which align well with the core principles of the circular economy model. When using hemp as a raw material for composites, the long bast fiber bundles are preferred for meshed/woven fiber laminates [5–7] or battens [8], while aggregates can be obtained from the xylemic core (hurd) for the fabrication of particulate composites such as particleboard (PB) [9–13].

The chemical composition and consistency of constituents along with their functional groups like hydroxyl, carboxyl, and phenolic groups, play pivotal roles in, e.g., matrix-reinforcement interaction, chemical reactivity, curing kinetics, cross-linking density, and resistance to environmental factors. Consequently, these factors significantly influence the quality and mechanical properties of bio-based composites. The presence of, i.e., oil, wax, and silica, has been demonstrated to adversely affect the self-bonding mechanisms of lignocellulosic materials during hot-pressing [14]. Additionally, soluble carbohydrates were found to significantly decrease the strength of wood-bonded cement panels [15] and may impede the setting time of bio-concretes [16].

The content and variability of extractives may also affect the interaction and compatibility with binders and coatings utilized for WBPs and innovative bio-composites. Bio-mineralized silica and wax are believed to diminish the wettability of particles, thereby reducing the bonding ability in rice (*Oryza sativa* L.) [17,18] and wheat (*Triticum sp* L.) [19] straw PB. The hydrophobicity of extractives also reduces wood surface permeability, negatively impacting the performance of waterborne coatings that rely on substrate permeability and access to the wood cell walls [20]. Acidic extractives have been shown to delay the curing reaction and final crosslinking of phenol resorcinol formaldehyde (PRF) [21] and polyurethane adhesives [22]. Bockel et al. [22] also demonstrated the degrading effect of starch on PRF and melamine-urea formaldehyde adhesives and showed that many extractives accelerate gel time. Meanwhile, the release of volatile extractives has been linked to issues of blowout and delamination in Western red cedar PB [23]. Additionally, the effects of extractives on adhesion may be exacerbated if they occur in interface areas, are concentrated, and/or the glueline is simultaneously exposed to multiple stressors [22]. Nevertheless, composites manufactured with tannin-formaldehyde adhesive showed lower formaldehyde emissions from Douglas fir (*Pseudotsuga menziesii* FRANCO) and Scots pine (*Pinus sylvestris* L.) heartwood compared to those from sapwood, suggesting that extractives may function as formaldehyde scavengers [24].

Much like established biomass-derived raw materials for WBPs such as wood [24], the composition of hemp hurd and various agricultural residues may vary based on genetics (cultivar), environmental conditions (soil, climate), plant maturity, and position within the plant [25]. Additionally, their chemical structure and compound proportions may be altered through various processes, including heat, steam, and/or enzymatic (pre)treatments [26,27]. As for hemp, the traditional prerequisite for enhanced separation of the bast fibers from the hurd during post-processing is referred to as 'field retting' (also dew-retting). Retting entails leaving the harvested hemp stems in the field, allowing the pectin-rich middle lamellas between fibers to degrade through a combination of enzymatic and microbial processes. While field retting is a cost-effective method, it is highly dependent on *in-situ* climatic circumstances and offers limited control. This dependence may result in significant variability in fiber quality [28]. Importantly, extending the retting duration beyond 22 days may induce alterations in the chemical composition and structural integrity of the hurd, potentially converting closed porosity to open porosity. Such transformations can substantially affect hurd density, water absorption kinetics, and thermal conductivity properties [16].

While the successful fabrication of various composites using hemp is reported, there is limited emphasis on comprehending and documenting the effects of the aforementioned factors that contribute to the inherent

variability of the raw hurd. Additionally, chemical analyses often focus on a specific representative cultivar and seldom compare different hurd and the effects of processing modalities.

A thorough documentation and understanding of the composition and influencing factors of bio-aggregate raw materials like hemp hurd are crucial for an informed hemp agronomy. This ensures that the raw material quality aligns with the specifications required for subsequent processing. Consequently, characterizing hemp hurd becomes a pivotal measure in successfully controlling and minimizing inherent variability within composite materials, preventing potential application failures. To complement the thermo-chemical characterization of reference material, Australian-grown 'Frog1' hemp hurd used in the fabrication of citric acid (CA)-bonded ultra-low-density hemp hurd particleboard [29], the present study examined the chemical composition and thermal stability of additional raw hemp hurd from selected hemp varieties harvested at different maturity stages and retting durations (Table 1). Furthermore, CA-resinated Frog1 particles (dried but not hot-pressed) were also included. The chemical composition and thermal stability analyses included pyrolysis-gas chromatography-mass spectrometry (Py-GC/MS) and thermogravimetric analysis (TGA), while Fourier-transform infrared (FTIR) spectroscopy was used to confirm the presence of functional groups.

Table 1: Hemp hurd origins and processing modalities

Origin	Variety	Treatment	Growing site	Sowing date	Harvest date	Retting	Post-harvest baling	Sampling date	Collection and storage
CSIRO [30]	Frog1	Early harvest	Smeaton, VIC	14/11/2020	24/2/2021	–	–	24/2/2021	Collected as straw from standing crop
		Late harvest			31/3/2021	–	–	31/3/2021	Collected as straw from standing crop
		Baled			18/4/2021	10 days	28/4/2021	23/6/2021	Bale outside until transfer to CSIRO (9/6/2021) > 2 weeks at 20°C and 50% RH > shipment to processing facility (23/6/2021)
	Han NE	Early harvest			24/2/2021	–	–	24/2/2021	Collected as straw from standing crop
		Late harvest			31/3/2021	–	–	31/3/2021	Collected as straw from standing crop
		Baled			31/3/2021	3–4 weeks	28/4/2021	23/6/2021	Bale outside until transfer to CSIRO (9/6/2021) > 2 weeks at 20°C and 50% RH > shipment to processing facility (23/6/2021)
		Retted			31/3/2021	5–6 weeks	–	Late May 2021	Collected as straw from the ground (unbaled swath)
AHMC	Frog1	Raw	–	–	–	–	–	n/a	Rinsed under running tap water (20°C) > dried at 65°C for 4 h > conditioned at 23°C and 65% RH
		Citric acid	–	–	–	–	–	n/a	Particles resinated with 59% concentrated citric acid at 30wt% (particle weight at 12% MC) > dried at 65°C for 4 h > conditioned at 23°C and 65% RH
		Autoclave	–	–	–	–	–		Particles treated in autoclave for 20 min at 130°C

2 Materials and Methods

Hemp hurd chips (*Cannabis sativa* L., AHMC 'Frog1' cultivar), from the Gippsland region in Victoria, Australia, were cleaned under tap water, dried at 60°C for 4 h, and conditioned at 23°C and 65% relative humidity (RH) until constant mass was achieved. The process of chip comminution and subsequent screening into particle size categories (PSC) followed the protocol reported in a prior study [9]. The material for the present study was sampled from the coarse (C) particle size fraction, as it was the most abundant. For the autoclave pre-treatment, PSC-C particles were subjected to 130°C for 20 min.

Anhydrous citric acid (CA) (C0759) was obtained from Sigma-Aldrich (Macquarie Park, Australia). PSC-C hurd was resinated with 59% concentrated CA solution applied at 30 wt%, followed by drying and conditioning as outlined for the Frog1 chips. Additional hemp stalks of 'Frog1' and 'Han NE' cultivars, with varying harvest times and retting durations, were sourced from the Commonwealth Scientific and Industrial Research Organization (CSIRO). A utility knife was employed to manually separate the hurd from the bast fibers. Table 1 provides a summary of the origins and processing methods, detailing harvest and retting times where available, while Fig. 1 visually represents the examined hemp hurd.

Figure 1: Examined raw hemp hurd. AHMC Frog1: hemp hurd chips (a); CSIRO Frog1: early harvest (b), late harvest (c), baled (d); CSIRO Han NE: early harvest (e), late harvest (f), baled (g), retted (h)

The operational and technical details for the Pyrolysis-gas chromatography-mass spectrometry (Py-GC/MS), Fourier-transform infrared spectroscopy (FTIR), and Thermogravimetric analysis (TGA) were applied as previously described [29] and are provided as Appendix A.

3 Results and Discussion

3.1 Pyrolysis-Gas Chromatography-Mass Spectrometry (Py-GC/MS)

Fig. 2 displays the Py-GC/MS chromatograms, along with the identified compounds and a summative analysis in Tables 2 and 3, respectively.

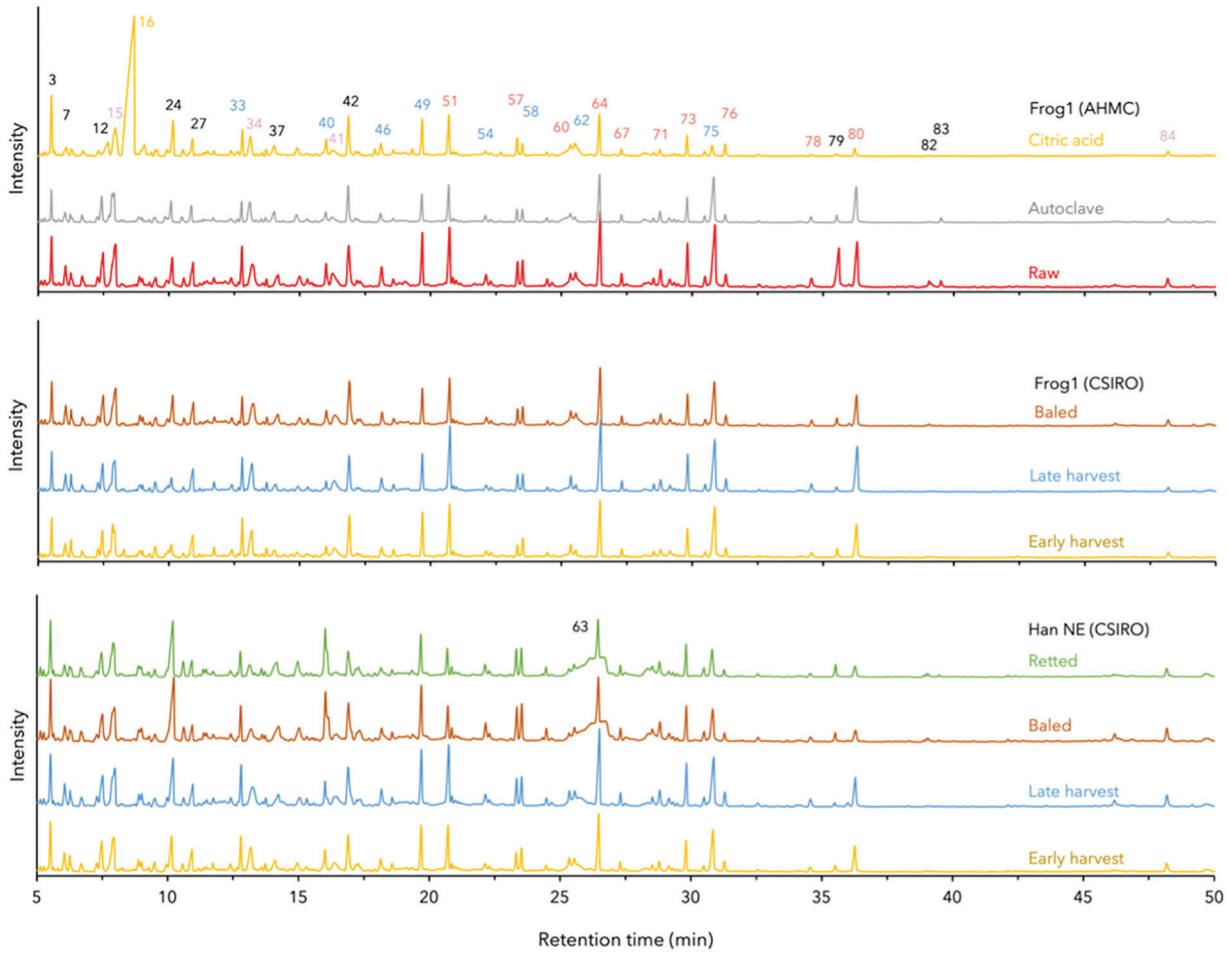

Figure 2: Comparison by superposition of hemp hurd Py-GC/MS chromatograms. Peak colors indicate compound origins: black = carbohydrate/nitrogen, blue = guaiacyl-lignin, red = syringyl-lignin, purple = extractives, yellow = citric acid

The release of compounds after pyrolysis of raw hemp hurd is primarily attributed to the lignin and carbohydrate components presented in Table 2. Compounds of smaller size, which tend to fragment easily at the start of pyrolysis, were excluded from the Py-GC/MS chromatograms due to the difficulty in their unambiguous differentiation. Lignin biosynthesis occurs through the polymerization of three phenylpropane units: *p*-coumaryl/hydroxyphenyl (H), coniferyl/guaiacyl (G), and sinapyl/syringyl (S) alcohol. The relative abundance of these monolignol units varies significantly depending on plant species, the structural location, and tissue type [25]. Softwood species are known to contain a higher proportion of

G-type lignin, whereas hardwood species comprise both G-type and syringyl (S)-type lignin, with S-units being more prevalent.

Table 2: Peak assignments and relative abundance of the principal compounds in hemp hurd released after Py-GC/MS

Peak	Pyrolysis product	Origin	AHMC Frog1			CSIRO Frog1			CSIRO Han NE			
			Raw	Citric acid	Autoclave	Early harvest	Late harvest	Baled	Early harvest	Late harvest	Baled	Retted
			Relative abundance (%)									
3	Furfural	CH	2.95	3.87	3.11	3.23	3.04	3.62	3.76	3.61	3.18	n.d.
7	2-Butanone	CH	1.60	0.71	1.58	1.56	1.71	1.99	1.86	1.90	1.12	n.d.
12	2(5H)-Furanone	CH	3.53	1.48	3.96	3.27	3.22	3.57	3.74	3.33	2.53	2.68
15	6-Oxa-bicyclo[3.1.0]hexan-3-one	E	5.68	4.29	3.17	2.03	5.59	6.94	6.67	5.49	4.21	5.33
16	2,5-Furandione, 3-methyl-(citraconic/itaconic anhydride)	CH	n.d.	34.95	n.d.	0.62	n.d.	n.d.	n.d.	n.d.	n.d.	n.d.
24	DL-Threonine, N-glycyl-	N	2.52	3.29	2.93	n.d.	1.64	3.34	4.67	n.d.	7.52	n.d.
27	1,2-Cyclopentanedione, 3-methyl-	CH	2.39	1.64	2.24	2.98	3.04	2.83	2.70	2.10	1.16	1.51
33	Guaiacol	G	2.61	1.63	2.33	3.53	2.75	2.31	2.89	3.04	2.19	1.98
34	Cyclopropyl carbinol	E	4.28	2.39	4.11	4.44	5.04	5.17	4.56	4.40	2.21	2.28
37	2,4(3H,5H)-Furandione, 3-methyl-	CH	1.44	1.46	1.77	1.17	1.08	2.23	1.82	1.87	2.88	3.32
40	Creosol	G	1.72	1.73	1.32	1.16	0.91	1.84	2.51	2.17	5.23	5.61
41	Catechol	E	2.57	1.30	n.d.	3.13	2.74	3.18	2.85	2.48	1.32	1.00
42	Benzofuran, 2,3-dihydro-	CH	4.39	3.46	5.49	5.49	4.22	6.29	4.65	4.86	3.92	2.89
46	1,2-Benzenediol, 3-methoxy-	G	1.81	1.22	1.25	1.34	1.59	1.43	n.d.	1.68	1.52	1.24
49	4-vinylguaiacol	G	3.78	2.40	3.25	4.44	3.30	3.16	4.01	3.91	4.04	3.24
51	Syringol	S	4.62	3.14	4.78	5.83	6.74	4.48	4.16	4.82	2.00	1.75
54	Vanillin	G	0.98	0.46	0.89	0.78	0.70	0.85	0.86	1.05	1.88	1.44
57	4-methylsyringol	S	n.d.	1.33	1.51	1.14	1.50	1.44	1.58	1.96	2.05	1.88
58	Isoeugenol (*trans*)	G	1.75	0.88	1.47	1.92	1.53	1.61	2.08	2.06	2.18	1.89
60	Benzene, 1,2,3-trimethoxy-5-methyl-	S	0.84	2.48	0.46	1.07	1.13	0.93	0.73	n.d.	0.83	1.08
62	Guaiacylacetone	G	1.82	2.23	0.35	0.57	0.37	0.49	0.53	0.75	1.37	2.12
63	1,3-Di-O-acetyl-.alpha.-.beta.-d-ribopyranose	CH	n.d.	n.d.	0.25	n.d.	n.d.	0.95	1.17	1.31	5.67	8.04
64	4-vinylsyringol	S	6.43	3.06	6.83	6.76	8.36	6.05	5.88	6.84	2.92	2.71
67	4-allylsyringol	S	0.80	0.44	0.81	0.77	n.d.	0.71	0.74	0.81	0.69	0.74
71	Syringaldehyde	S	1.32	0.57	1.58	0.98	1.30	1.18	1.00	1.28	1.72	1.48
73	4-propenylsyringol (*trans*)	S	3.14	1.40	3.13	2.87	3.54	2.81	2.81	3.19	2.12	2.15
75	Coniferyl alcohol	G	8.00	1.08	8.71	8.47	8.04	6.54	5.93	5.91	3.20	2.86

(Continued)

Table 2 (continued)

Peak	Pyrolysis product	Origin	AHMC Frog1			CSIRO Frog1			CSIRO Han NE			
			Raw	Citric acid	Autoclave	Early harvest	Late harvest	Baled	Early harvest	Late harvest	Baled	Retted
			Relative abundance (%)									
76	Syringylacetone	S	1.13	0.87	0.94	1.06	1.24	1.02	1.04	1.16	0.57	0.56
78	Sinapyl alcohol (*cis*)	S	0.84	n.d.	0.97	0.68	0.96	0.70	0.62	0.78	0.43	0.38
79	Palmitic acid	CH	4.46	n.d.	0.99	0.92	0.47	0.74	0.61	n.d.	0.53	1.01
80	Sinapyl alcohol (*trans*)	S	4.84	0.72	6.87	4.80	6.68	3.79	3.04	2.73	1.04	1.20
82	Oleic Acid	CH	0.24	n.d.	n.d.	n.d.	n.d.	n.d.	n.d.	n.d.	n.d.	n.d.
83	Octadecanoic acid	CH	0.43	n.d.	n.d.	n.d.	n.d.	n.d.	n.d.	n.d.	n.d.	n.d.
84	(E)-3,3'-Dimethoxy-4,4'-dihydroxystilbene	E	0.78	0.55	0.66	0.73	0.57	0.71	1.01	1.04	1.22	0.95

Note: Origin: CH = carbohydrate; N = Protein; G = guaiacyl-lignin; S = syringyl-lignin; E = extractives, n.d. = not determined.

Table 3: Summative chemical composition of hemp hurd identified by Py-GC/MS

Variety	AHMC Frog1			CSIRO Frog1			CSIRO Han NE			
Treatment	Raw	Citric acid	Autoclave	Early harvest	Late harvest	Baled	Early harvest	Late harvest	Baled	Retted
Total derived extractives (%)	13.57	10.59	9.01	12.91	15.08	16.70	17.18	19.64	19.79	10.04
Total derived carbohydrate (%)	33.70	59.19	37.46	31.54	27.37	35.83	35.82	29.88	38.19	45.12
H-unit lignin (%)	2.57	2.41	1.34	2.95	3.20	2.78	3.39	2.40	2.90	1.16
G-unit lignin (%)	24.52	12.34	20.94	24.99	21.30	20.20	20.61	22.84	21.55	24.08
S-unit lignin (%)	25.27	15.49	29.16	27.06	32.82	24.13	22.64	24.90	17.15	17.67
Total derived lignin (%)	52.36	30.24	51.44	55.00	57.32	47.11	46.64	50.14	41.60	42.91
H/G/S ratio	5:47:48	8:41:51	3:41:57	5:45:49	6:37:57	6:43:51	7:44:49	5:46:50	7:52:41	3:56:41
S/G ratio	1.03	1.26	1.39	1.08	1.54	1.19	1.10	1.09	0.80	0.73
L/C ratio	1.55	0.51	1.37	1.74	2.09	1.31	1.30	1.68	1.09	0.95

Note: Lignin units: H = *p*-coumaryl/hydroxyphenyl, G = coniferyl/guaiacyl, S = sinapyl/syringyl.

The Py-GC/MS analysis showed a notable low abundance of H-unit lignin in all hemp hurd samples. This is consistent with lower concentrations of H-unit lignin for both softwood and hardwood species in general, as well as non-woody biomass lignins of bast fibers from, i.e., hemp, flax, and jute [31]. In the same study, the Py-GC/MS analysis of hemp bast fibers revealed a H/G/S ratio of 9:51:40, which closely resembled the 7:52:41 ratio observed in baled Han NE hurd and to some extent, the 3:56:41 ratio of retted Han NE. In the present study, all other hemp hurd samples displayed inverse configurations, characterized by reduced proportions of G-unit lignin and an increased prevalence of S-unit lignin. The total lignin derivative content initially increased with maturity but subsequently decreased with prolonged storage and/or retting for the CSIRO Frog1 and Han NE varieties. The lower lignin levels in the baled samples could result from compression and mechanical damage to the biomass during the baling process [32], which can accelerate the exposure of lignin to environmental factors. Additionally, increased moisture retention inside the bale may increase anaerobic microbial activity and

enhance the activity of lignin-degrading enzymes produced by fungi and bacteria [33,34]. Interestingly, the S-type lignin increased by 21.29%, whereas G-type lignin decreased by 14.77% in early to late harvest CSIRO Frog1, respectively. Conversely, both S- and G-type lignin increased by 9.98% and 10.82%, respectively, in Han NE.

After undergoing autoclave treatment, the total lignin content of the raw AHMC Frog1 decreased only moderately by 1.76%. However, the abundance of monolignols displayed a significant shift, with a 15.39% increase in S-unit content and a 14.60% decrease in G-unit content in autoclaved AHMC Frog1. Increased levels of S-units and elevated S/G ratios typically result in improved pulping efficacy and signify faster delignification rates due to the heightened reactivity of S-lignin in alkaline conditions [35]. In the current study, only the S/G ratios of CSIRO Frog1 were influenced by maturity (1.08 to 1.54), whereas the ratios of Han NE remained constant (1.10 to 1.09). Raw AHMC Frog1 displayed the most balanced S/G ratio of 1.03, whereas the application of autoclave treatment resulted in an increase to 1.39, attributable to the G-unit breakdown. The intrinsic variability in lignin composition in biomass, along with different methodologies for determining the S/G ratio, can present challenges for the comparison of S/G ratios in the literature. Nevertheless, it is noteworthy that the results from this study align with reported S/G ratios of hemp hurd, namely 0.8 [31] and 1.42, and are generally lower when compared to S/G ratios other non-woody biomass types, such as jute (2.1) [35], or abaca, sisal, and jute (2.9, 3.4, and 1.7, respectively) [31].

The lignin-to-carbohydrate (L/C) ratio is a useful indicator of biomass cell wall composition and can provide insight into the utility for industrial processes i.e., composites, biofuels, or pulping. A higher L/C ratio is typically associated with tougher and more rigid plant material, while a lower ratio suggests a more easily digestible and softer material. In the total derivate count, carbohydrate presence is inverse proportional to lignin abundance. As a result, mature CSIRO Frog1 and Han NE with high lignin content exhibited high L/C ratios of 2.09 and 1.68, respectively, while L/C ratios decreased in baled samples with reduced lignin content to 1.31 and 0.95, and 1.09 (retted), respectively.

CA-resinated AHMC hemp hurd was the only sample comprising an added substance. Studies on the thermal degradation of CA determined a melting point between 153°C [36] and 160°C [37], and decomposition around 175°C [38] or 203°C [37]. Prolonged heating of CA leads to the formation of intermediate compounds, namely aconitic acid (*cis* and *trans*) followed by aconitic anhydride (*cis* and *trans*). Through complex dehydration and decarboxylation reactions, citraconic and/or itaconic anhydrides are ultimately formed as the end products. These isomeric compounds are difficult to separate using chromatographic techniques and may be frequently reported as a combined sum of both isomers [37,39]. Exposure to citraconic anhydride is linked to respiratory hypersensitivity reactions i.e., contact sensitization, and occupational asthma [39]. Given their close structural relationship, it is reasonable to consider both compounds as respiratory sensitizers. Citraconic and/or itaconic anhydride was the predominant compounds (34.95%) in CA-resinated hemp hurd. Although citraconic/itaconic anhydride is not a carbohydrate, it was classified by the Pyris analysis software as ‘carbohydrate originated’, which caused a significant alteration of the samples’ L/C ratio to 0.51, in contrast to the 1.55 and 1.37 observed in raw and autoclaved Frog1, respectively. Excluding citraconic/itaconic anhydride from the total carbohydrate count led to a hypothetical L/C ratio of 1.27.

Extractives, such as tannins and phenolic compounds, may disrupt matrix-to-fiber bonding mechanisms in lignocellulosic composite materials [40]. This can be attributed to the chemical reaction of these compounds with the alkaline environment of the matrix, resulting in acidic conditions that could impede sufficient bonding. In bio-based concretes, solubles like pectins, proteins, and lipids may leach into the mixture [16], potentially altering setting time, strength, and the composition of the final product. The present study showed that extractive derivatives increased with maturity to 15.08% and 19.64% in late

harvest CSIRO Frog1 and Han Ne, respectively, compared to 13.57% in raw AHMC Frog1. The application of retting and autoclave treatment led to a notable decrease in extractive content in both Han NE and AHMC Frog1 by 48.88% and 33.60%, respectively.

The Py-GC/MS analysis revealed a strong consistency in the identified compounds among the raw hemp hurd samples, despite variations in their abundance. An exception was observed in Han NE, where the presence of 1,3-Di-O-acetyl-α-β-d-ribopyranose was more pronounced, especially in the baled and retted samples with extended retting durations (peak 63). The origin of citraconic/itaconic anhydride was caused by the resination of AHMC Frog1 using CA. The same sample also showed a notable reduction in lignin derivatives (peaks 41, 49, 64, 71, 73, 75, 79, 80) and the absence of fatty acids (peaks 79, 82, 83) compared to the raw AHMC Frog1. A reduction in fatty acids was also noted during the creation of CA-bonded ultra-low density hemp hurd PB [29]. These observations suggest potential reactions and structural changes during thermal degradation, which could enhance the bonding mechanisms and particle adhesion. The same fatty acids were either notably less prevalent (peak 79) or not determined at all (peaks 82 and 83) in CSIRO Frog1 and Han NE.

3.2 Fourier-Transform Infrared (FTIR) Spectroscopy

FTIR spectra are depicted in Fig. 3 and the main FTIR absorption bands for each spectrum were numbered and functional groups and attributable components summarized in Table 4.

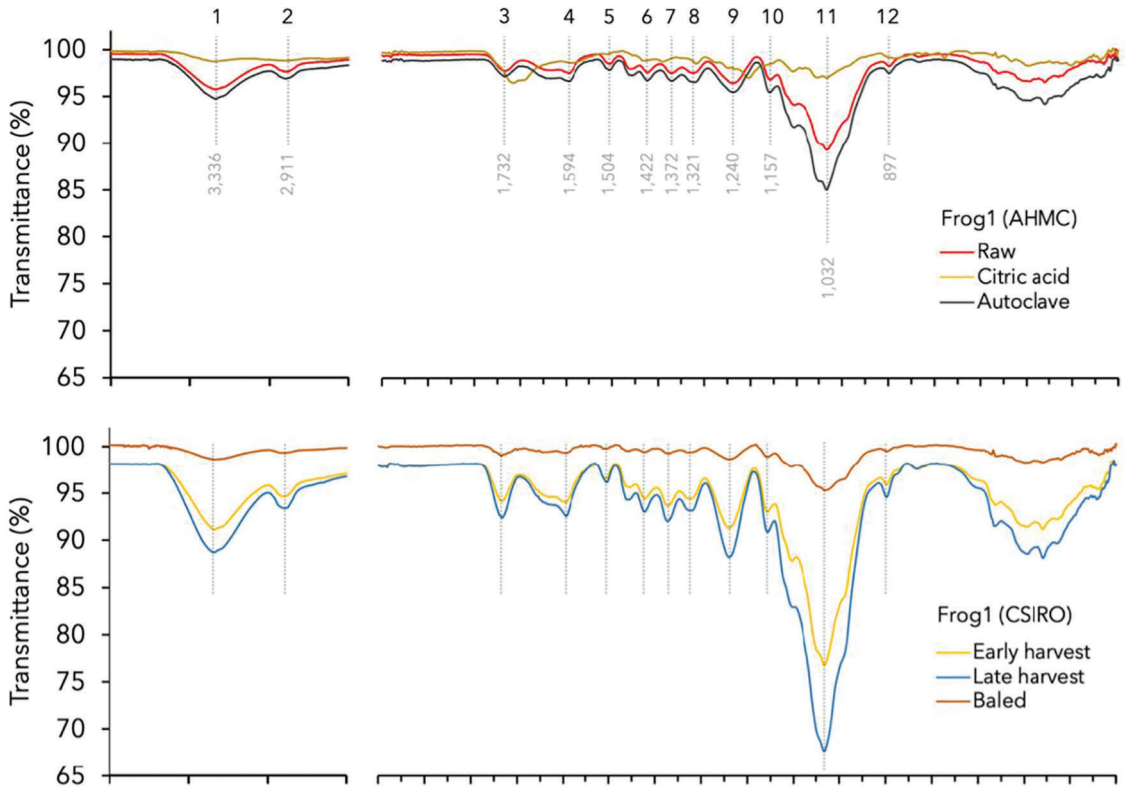

Figure 3: (Continued)

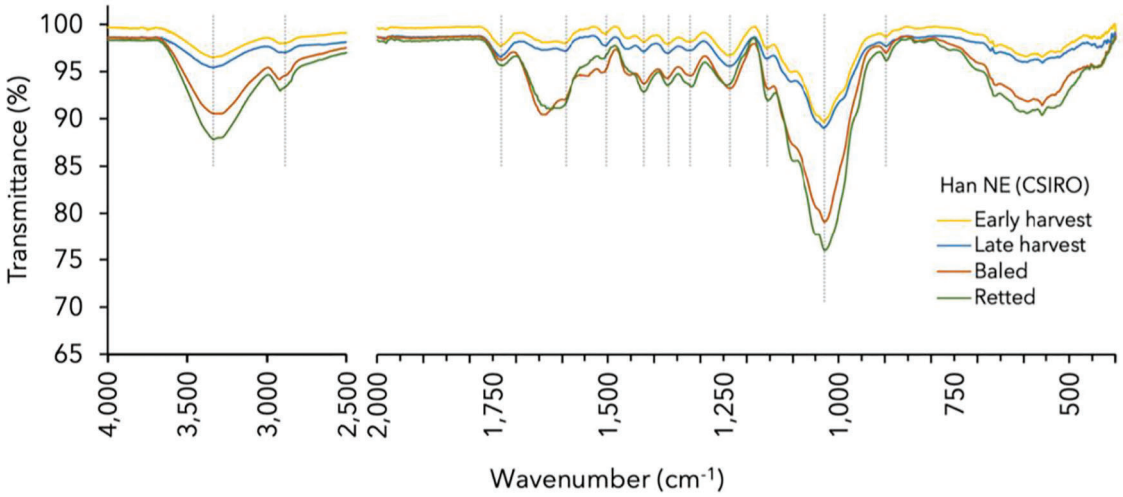

Figure 3: FTIR spectra of hemp hurd with assigned bands and mean for corresponding wavenumber ranges (Table 4)

Table 4: Common wavenumber characteristics of absorption bands observed in hemp hurd [26,41–44]. Band numbers refer to assigned bands in Fig. 3

Wavenumbers (cm^{-1})	Assignments, functional groups, and polymers	Band
3334–3337	O-H stretching, (lignin, polysaccharides)	1
2899–2923	C-H stretching of methyl-and methylene groups (cellulose, hemicellulose, polysaccharides, and wax)	2
1730–1734	C=O unconjugated stretching in acetyl groups (hemicellulose, lignin, pectin, fatty acids)	3
1594–1595	C=C aromatic ring vibrations and C=O stretching (lignin)	4
1504–1505	C=C benzene ring vibration (lignin)	5
1422–1423	HCH and OCH in-plane bending vibration, CH_2 symmetric bending, C=C stretching in aromatic groups (cellulose, hemicellulose pectin, lignin)	6
1371–1373	C-H deformation in (crystalline cellulose, hemicellulose)	7
1317–1326	C=O vibration in syringyl derivates and cellulose (lignin, cellulose)	8
1236–1244	Guaiacyl ring and C-O stretch in lignin and xylan (lignin, hemicellulose)	9
1155–1159	C-O-C vibration and C-O stretch in ester groups (cellulose, hemicellulose, lignin)	10
1030–1034	C-C, C-OH, C-H ring and side group vibration (cellulose, hemicellulose, lignin, pectin)	11
897–898	C-H deformation and glycosidic linkage (amorphous cellulose, hemicellulose, polysaccharides)	12

The FTIR analysis indicated that spectral features of the hemp hurd exhibited great resemblance to those of lignocellulosic polymers reported in the literature. The primary spectral alterations observed among the different hemp samples were changes in band intensities. The broad peaks observed around 3340 cm^{-1} (O-H stretching; 1) and 2908 cm^{-1} (C-H stretching; 2) are pure bands and indicating the presence of hydroxyl groups in holocellulose and other polysaccharides. Typical cellulose bands were observed at 1322 cm^{-1} (CH_2 vibrations; 8), 1157 cm^{-1} (C-O-C asymmetrical stretching, cellulose/hemicellulose; 9), and 897 cm^{-1} (β-glycosidic bonds symmetrical ring-stretching mode, amorphous cellulose; 12). Meanwhile, hemicelluloses were identified by peaks at 1733 cm^{-1} (conjugated C=O in xylans; 3), 1373 cm^{-1} (C-H deformation; 7), and 1157 cm^{-1} (C-O-C vibrations; 10). In the fingerprint region (<1500 cm^{-1}), the spectral analysis revealed the existence of a dominant peak at 1032 cm^{-1} (11). Due to the peak's potential to match multiple vibration modes in carbohydrates and lignin, its direct attribution to a specific functional group was not feasible [45]. The lack of specific bonding (specific wavenumber) of hemicellulose was previously stated by Viel et al. [46] who also noted the close resemblance of the hemicellulose monomers to cellulose units and pectin as well as lignin monomers. Consequently, this complex band merely provided evidence for the presence of one or more of these components.

Hemp hurd comprises guaiacyl-syringyl (hardwood) lignin, indicated by absorbance around 1270 cm^{-1} and 1230 cm^{-1} for guaiacyl and 1315 cm^{-1} for syringyl, respectively [45,47]. However, the present study detected distinct guaiacyl-lignin frequencies between 1236–1244 cm^{-1} and, consistent with Gandolfi et al. [47], the 1270 cm^{-1} was absent. Other characteristic lignin bands were identified around 1504 cm^{-1} (benzene ring vibration; 5), 1423 cm^{-1} (guaiacyl and syringyl condensed nuclei; 6), 1322 cm^{-1} (aromatic C-O stretching (syringyl); 8) and 1240 cm^{-1} (aromatic C-O stretching (guaiacyl); 9) [47,48].

The autoclave treatment was found to enhance the absorbance of Frog1 without altering the spectral pattern of the raw equivalent. Contrarily, CA-resinated Frog1 exhibited a distinct FTIR spectra with reduced intensities in peaks 1, 2, and 11, peak shifts and attenuation in peaks 4, 8, 9, and 12, and the absence of peaks 5, 7, and 10. These changes were attributed to partial reactions during pyrolysis and the higher concentration of non-cellulosic CA compounds.

The study found that CSIRO Frog1 exhibited much greater absorbance than Han NE despite great similarities in spectral patterns. The peak intensities increased with crop maturity in both hemp varieties, with early harvest samples showing lower peak intensities compared to late harvest samples. Furthermore, baling, and retting treatments amplified overall signal intensities in Han NE indicating higher concentrations of the functional groups in the sample.

A minor peak shift from 2900 cm^{-1} (C-H symmetrical stretching in cellulose and hemicellulose) to 2920 cm^{-1} and 2923 cm^{-1}, respectively, suggested the degradation of polysaccharides and presence of lignin (stretching of lignin aromatic hydrocarbon, methoxy and methylene groups). A pronounced peak broadening and shift occurred from 1595 cm^{-1} (presence of aromatic ring in lignin; 4) to 1639 cm^{-1} and 1623 cm^{-1}, respectively, associated with the C=O stretching in conjugated carbonyl of lignin or absorbed water in cellulose [26]. Stronger peak intensities around 1373 and 1157 cm^{-1} indicate a higher concentration of carbohydrates in samples that were more mature, retted, or stored for longer periods (baled). Conversely, baling had the opposite effect in CSIRO Frog1, resulting in much greater transmission and pronounced peak attenuation.

3.3 Thermogravimetric Analysis (TGA)

The thermogravimetric (TG in wt.%) and differential TG (DTG in mg/min) profiles of the raw hurd are shown in Fig. 4a–f while Table 5 summarizes the thermal stability details.

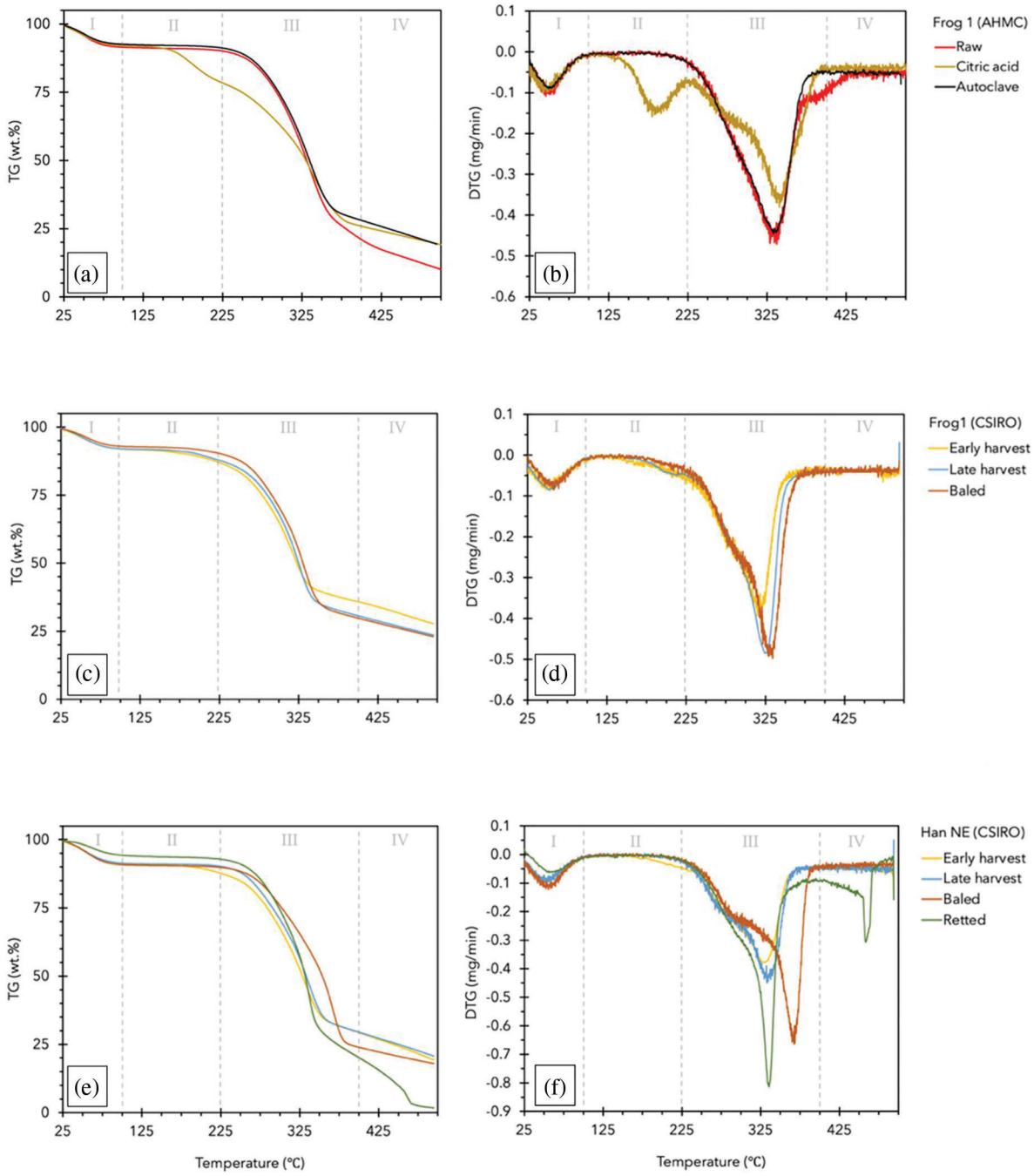

Figure 4: Thermogravimetric (TG) and differential TG (DTG) profiles of hemp hurd: Frog1 (AHMC) (a, b), Frog1 (CSIRO) (c, d), and Han NE (CSIRO) (e, f). Phases I–IV indicate the most prominent degradation stages

The thermograms exhibited the common dehydration and de-polymerization processes typical for lignocellulosic biomass. A predominantly bimodal degradation pattern was observed in most samples, with additional peaks occurring in CA-resinated Frog1 and retted Han NE. Until approximately 100°C (phase I) the mass loss of 5.7% to 9.2% was primarily attributed to moisture loss and the decomposition

of low molecular weight compounds (i.e., extractives). The sample weight then remained stable (phase II) until the second degradation stage (phase III), which commenced above 200°C and typically ended below 340°C. During phase III, the most significant weight loss (56% to 81.3%) occurred due to the initial breakdown of pectins and amorphous hemicelluloses (200°C–260°C). The removal of non-cellulosic components led to the formation of a more structurally ordered cellulose, which increased its thermal stability and was observed as the main peak within a temperature range of 240°C to 350°C [49–51]. The DTG curves of retted and baled Han NE showed two distinct peaks in phase III indicating depolymerization at approximately 290°C (pectins, hemicelluloses) and 337°C and 369°C (cellulose), respectively (Fig. 4f). However, the complexity of these reactions may prevent a clearly defined sequential degradation process, as suggested by the indistinct peak separation (shoulder peak) in the DTG curves of both Frog1 varieties (Fig. 4b,d).

Table 5: Thermal stability of raw hemp hurd

Phase	Variable	AHMC Frog1			CSIRO Frog1			CSIRO Han NE			
		Raw	Citric acid	Autoclave	Early harvest	Late harvest	Baled	Early harvest	Late harvest	Baled	Retted
I	Weight loss (%)	8.2	7.4	7.4	7.9	7.9	6.6	8.8	8.5	9.2	5.4
	DTG peak (°C)	46.7	50.1	50.4	54.0	59.7	59.0	73.6	59.8	56.8	58.1
II	Weight loss (%)	–	14.3	–	–	–	–	–	–	–	–
	DTG peak (°C)	–	180.9	–	–	–	–	–	–	–	–
III	Weight loss (%)	81.3	56.1	68.1	56.0	62.6	63.7	63.4	63.2	69.0	73.7
	DTG peak (°C)	338.3	341.7	334.3	315.5	326.8	334.8	330.3	333.6	367.9	336.5
IV	Weight loss (%)	–	–	–	–	–	–	–	–	–	17.2
	DTG peak (°C)	–	–	–	–	–	–	–	–	–	459.5
Total weight loss (%)		89.5	77.9	75.5	63.9	70.5	70.3	72.2	71.7	78.2	96.3
Residual weight (%)		10.5	22.1	24.5	36.1	29.5	29.7	27.8	28.3	21.8	3.7
Weight loss at 100°C (%)		8.5	7.8	7.4	8.1	8.0	7.1	8.8	8.6	9.2	5.7
T-5% (°C)		54.2	55.4	59.5	59.0	59.8	66.3	56.9	57.8	56.4	82.6
T-10% (°C)		227.1	163.6	242.5	183.6	198.2	228.8	188.1	228.9	216.7	256.5
T-20% (°C)		281.2	213.2	284.3	264.5	271.2	278.9	270.2	277.9	288.3	288.3
T-60% (°C)		343.5	347.1	347.9	348.9	336.6	341.9	342.7	345.7	364.4	338.7
T max (°C)		338.3	341.7	334.3	315.5	326.8	334.8	330.3	333.6	367.9	336.5

The rapid mass loss observed during phase III for baled and retted Han NE can be attributed to the field retting durations of 3–4 and 5–6 weeks, respectively. In the initial retting stages, pectins and some hemicelluloses are degraded in the thin middle lamellas (10 nm) followed by primary cell walls (10 nm). This promotes separation of the bast fibers but does not cause structural changes in the hurd in the first 22 days of retting [16]. During this stage, the relative proportion of cellulose and lignin in the biomass typically increase [52] which may explain the greater thermal resistance of baled Han NE in phase III. With prolonged retting, the middle lamellas and primary walls are removed, gradually exposing cellulose, which is subsequently metabolized during the attack on the much thicker secondary walls (250 nm). After 42 days of retting, a considerable reduction in the secondary wall structures of hemp hurd tissue occurred [16].

The removal of hemicelluloses may have contributed to a lower moisture uptake of retted Han NE, leading to a lower initial EMC. This could explain the notable lower mass loss of 5.7% in phase I. However, extended retting may have caused additional deterioration of the cell wall structure allowing for a rapid pyrolysis of cellulose and lignin components. Due to diverse chemical bond activities, lignin exhibits increased thermal stability [49] and a broad degradation temperature range, with reported values ranging from 280°C to 500°C [51] and even 100°C to 900°C [50]. The chemical modification in retted Han NE hurd resulted in an additional decomposition step (phase IV) at around 460°C. This led to a residual weight of 3.7%, the lowest observed in the study.

Raw and autoclaved AHMC Frog1 exhibited comparable decomposition patterns. However, the breakdown of raw Frog1 persisted around 400°C, resulting in a substantially lower residue of 10.5% compared to 24.5% and 22.1% for autoclaved and CA-resinated Frog1, respectively. An additional peak at 180.0°C confirmed the previously mentioned thermal breakdown of CA between 175°C and 203°C [37,38].

4 Conclusion

Hemp hurd samples with different provenance, maturity stage, and retting protocol, respectively, were subjected to Py-GC/MS, FTIR, and TG analyses and compared to hemp hurd used in the fabrication of citric acid-bonded ultra-low-density hemp hurd particleboard.

All the samples analyzed adhered to the previously reported S/G ratios for hemp hurd, which were generally lower than those of other non-woody biomass types. The study revealed variations in the total derived lignin content among different cultivars, with an increase observed in relation to maturity and a decrease associated with prolonged retting. As a result, the lignin-to-carbohydrate (L/C) ratio, which serves as a valuable indicator of biomass cell wall composition, mirrored the trend seen in the total lignin proportion. The concentration of potentially disruptive extractive substances reached its peak in mature hurd but significantly decreased with prolonged retting—an outcome that was similarly observed during autoclave treatment.

Notable differences between the cultivars included the absence of fatty acids in the CSIRO samples. The contribution of fatty acids to the enhancement of adhesion in lignocellulosic materials has been acknowledged, and this factor might render certain hemp cultivars unfavorable in the selection for binderless (self-bound) composites relying predominantly on auto-adhesion.

While FTIR signals confirmed similar functional groups, variations in peak intensities indicated substantial differences among cultivars, including carbohydrate levels related to maturity and retting. These differences may impact the availability of hydroxyl groups, a favorable attribute affecting the bonding mechanism in citric acid-bonded biobased hemp composites. Conversely, higher carbohydrate proportions might compromise the dimensional stability of these composites.

The predominantly bimodal degradation observed during TGA between most hurd samples was consistent with common lignocellulosic biomass. However, the results also highlighted differences between the cultivars and processing modalities. While shorter retting duration initially enhanced the thermal resistance of the hurd, prolonged retting (i.e., structural breakdown) resulted in accelerated degradation and significantly reduced residual mass of CSIRO Han NE. Notably, unmodified raw AHMC Frog1, utilized in the production of citric acid-bonded hemp particleboard, exhibited the second lowest residual mass. Autoclave treatment of the same hurd resulted in a higher residual mass, suggesting the formation of more thermally stable compounds.

It should be noted that the effect of field retting on hemp biomass is predominantly influenced by a multitude of uncontrollable environmental factors. Despite its cost-effectiveness, the dependency on variable microbial activity poses a significant challenge to achieving consistency. Additionally, the intrinsic chemical composition of industrial hemp samples is affected by several factors, including variety, agronomic practices, specimen location within the plant, and fiber extraction and processing technologies. Consequently, the findings of this study emphasize the role of cultivar, maturity, and processing modalities in shaping the thermo-chemical properties of hemp hurd. Further research should explore the significance of raw material variability and examine the extent to which the observed differences impact physico-mechanical properties. This will ensure that the raw material characteristics align with the specifications required for applications such as biobased hemp hurd composites.

Acknowledgement: Recognition is given to Darren Christie (AHMC, VIC) for supplying decorticated raw Frog1. The authors also extend their gratitude to Stuart Gordon and Menghe Malcom Miao (CSIRO) for their provision of additional raw Frog1 and Han NE hemp.

Funding Statement: This study received financial support from the Australian government through the Australian Centre for International Agricultural Research (ACIAR) Initiative under Project No. FST/2016/151. The primary author was a recipient of a Melbourne University Research Scholarship and received financial assistance from the Dr. Albert Shimmins Fund.

Author Contributions: Johannes Fehrmann took part in conceptualization, data curation, formal analysis, investigation, methodology, project administration, software, validation, visualization, writing—original draft, and writing—review and editing. Benoit Belleville took part in conceptualization, funding acquisition, project administration, resources, supervision, validation, and writing—review and editing. Barbara Ozarska involved in conceptualization, funding acquisition, project administration, resources, supervision, validation, and writing—review and editing. Maya Ismayati took part in investigation, and writing—review and editing. Wahyu Dwianto involved in resources and writing—review and editing. All authors reviewed the results and approved the final version of the manuscript.

Availability of Data and Materials: The datasets generated during and/or analyzed during the current study are available from the corresponding author on reasonable request.

Conflicts of Interest: The authors declare that they have no conflicts of interest to report regarding the present study.

References

1. Montford S, Small E. A comparison of the biodiversity friendliness of crops with special reference to hemp (*Cannabis sativa* L.). J Int Hemp Assoc. 1999;56(6):53–63.
2. Petersen J-E, Elbersen B, Wiesenthal T, Feehan J, Eppler U. Estimating the environmentally compatible bioenergy potential from agriculture. Copenhagen, Denmark: European Environment Agency; 2007. p. 138.

3. Ahmed ATMF, Islam MZ, Mahmud MS, Sarker ME, Islam MR. Hemp as a potential raw material toward a sustainable world: a review. Heliyon. 2022;8(1):e08753. doi:10.1016/j.heliyon.2022.e08753.
4. Crini G, Lichtfouse E, Chanet G, Morin-Crini N. Applications of hemp in textiles, paper industry, insulation and building materials, horticulture, animal nutrition, food and beverages, nutraceuticals, cosmetics and hygiene, medicine, agrochemistry, energy production and environment: a review. Environ Chem Lett. 2020;18:1451–76. doi:10.1007/s10311-020-01029-2.
5. Corbin AC, Soulat D, Ferreira M, Labanieh AR. Influence of process parameters on properties of hemp woven reinforcements for composite applications: mechanical properties, bias-extension tests and fabric forming. J Nat Fiber. 2022;19:1–13. doi:10.1080/15440478.2020.1761925.
6. Awais H, Nawab Y, Anjang A, Akil HM, Abidin Z, Shukur M. Effect of fabric architecture on the shear and impact properties of natural fibre reinforced composites. Compos Part B: Eng. 2020;195:108069. doi:10.1016/j.compositesb.2020.108069.
7. Hernandez-Estrada A, Müssig J, Hughes M. The impact of fibre processing on the mechanical properties of epoxy matrix composites and wood-based particleboard reinforced with hemp (*Cannabis sativa* L.) fibre. J Mater Sci. 2022;57(3):1738–54. doi:10.1007/s10853-021-06629-z.
8. Liao J, Zhang S, Tang X. Sound absorption of hemp fibers (*Cannabis Sativa* L.) based nonwoven fabrics and composites: a review. J Nat Fiber. 2022;19:1–13. doi:10.1080/15440478.2020.1764453.
9. Fehrmann J, Belleville B, Ozarska B. Effects of particle dimension and constituent proportions on internal bond strength of ultra-low-density hemp hurd particleboard. Forests. 1967;13(11):1967. doi:10.3390/f13111967.
10. Auriga R, Pedzik M, Mrozowski R, Rogozinski T. Hemp shives as a raw material for the production of particleboards. Polymers. 2022;14(23):5308. doi:10.3390/polym14235308.
11. Tupciauskas R, Rizhikovs J, Andzs M, Bikovens O. Influence of manufacturing conditions on binder-less boards from steam-exploded hemp shives and wheat straw. Materials. 2022;15(9):3141. doi:10.3390/ma15093141.
12. Alao P, Tobias M, Kallakas H, Poltimäe T, Kers J, Goljandin D. Development of hemp hurd particleboards from formaldehyde-free resins. Agron Res. 2020;18(Special Issue 1):679–88. doi:10.15159/ar.20.127.
13. Fehrmann J, Belleville B, Ozarska B, Gutowski WS, Wilson D. Influence of particle granulometry and panel composition on the physico-mechanical properties of ultra-low-density hemp hurd particleboard. Polym Compos. 2023;44(11):7363–83. doi:10.1002/pc.27631.
14. Marbun SD, Dwianto W, Meliala SBPS, Widyorini R, Augustina S, Hiziroglu S. Dimensional stability mechanisms of binderless boards by heat or steam treatment: a review. Cellulose. 2023;30:8571–93. doi:10.1007/s10570-023-05429-9.
15. Sandermann W, v Dehn U. Einfluß chemischer Faktoren auf die Festigkeitseigenschaften zementgebundener Holzwolleplatten. Holz Roh Werkst. 1951;9(3):97–101 (In German). doi:10.1007/BF02615547.
16. Arufe S, Hellouin de Menibus A, Leblanc N, Lenormand H. Effect of retting on hemp shiv physicochemical properties. Ind Crops Prod. 2021;171:113911. doi:10.1016/j.indcrop.2021.113911.
17. Kurokochi Y, Saito Y. Heat treatment to increase self-bonding property of binderless boards manufactured from rice straw. IOP Conf Series: Earth Environ Sci. 2022;1063(1):12002. doi:10.1088/1755-1315/1063/1/012002.
18. Kurokochi Y, Sato M. Steam treatment to enhance rice straw binderless board focusing hemicellulose and cellulose decomposition products. J Wood Sci. 2020;66(1):7. doi:10.1186/s10086-020-1855-8.
19. Chougan M, Ghaffar SH, Mijowska E, Kukułka W, Sikora P. High-performance polylactic acid compressed strawboard using pre-treated and functionalised wheat straw. Ind Crops Prod. 2022;184:114996. doi:10.1016/j.indcrop.2022.114996.
20. Wu Y, Zhang H, Yang L, Wang S, Meng Y. Understanding the effect of extractives on the mechanical properties of the waterborne coating on wood surface by nanoindentation 3D mapping. J Mater Sci. 2021;56(2):1401–12. doi:10.1007/s10853-020-05347-2.
21. Özparpucu M, Windeisen-Holzhauser E, Wegener G, Richter K. A new analytical approach to investigate the influence of wood extracts on the curing properties of phenol-resorcinol-formaldehyde (PRF) adhesives. Wood Sci Technol. 2022;56(2):349–65. doi:10.1007/s00226-022-01364-3.

22. Bockel S, Mayer I, Konnerth J, Harling S, Niemz P, Swaboda C, et al. The role of wood extractives in structural hardwood bonding and their influence on different adhesive systems. Int J Adhes Adhes. 2019;91:43–53. doi:10.1016/j.ijadhadh.2019.03.001.
23. Shmulsky R, Jones PD. Forest products and wood science: an introduction. 6 ed. Hoboken, NJ, USA: Wiley-Blackwell; 2011.
24. Roffael E. Significance of wood extractives for wood bonding. Appl Microbiol Biotechnol. 2016;100(4):1589–96. doi:10.1007/s00253-015-7207-8.
25. Xu F, Yu J, Tesso T, Dowell F, Wang D. Qualitative and quantitative analysis of lignocellulosic biomass using infrared techniques: a mini-review. Appl Energ. 2013;104:801–9. doi:10.1016/j.apenergy.2012.12.019.
26. Alao PF, Marrot L, Burnard MD, Lavrič G, Saarna M, Kers J. Impact of alkali and silane treatment on Hemp/PLA composites' performance: from micro to macro scale. Polymers. 2021;13(6):851. doi:10.3390/polym13060851.
27. Väisänen T, Batello P, Lappalainen R, Tomppo L. Modification of hemp fibers (*Cannabis Sativa* L.) for composite applications. Ind Crops Prod. 2018;111:422–9. doi:10.1016/j.indcrop.2017.10.049.
28. Liu M, Thygesen A, Summerscales J, Meyer AS. Targeted pre-treatment of hemp bast fibres for optimal performance in biocomposite materials: a review. Ind Crops Prod. 2017;108:660–83. doi:10.1016/j.indcrop.2017.07.027.
29. Fehrmann J, Belleville B, Ozarska B, Ismayati M, Dwianto W. Effects of mat composition and pressing time on citric acid-bonded ultra-low-density hemp hurd particleboard. Ind Crops Prod. 2024;210:118070. doi:10.1016/j.indcrop.2024.118070.
30. Gordon S, Miao M. Developing technical plans for processing Australian industrial hemp straw. Australia: AgriFutures Australia; 2022. p. 40.
31. del Río JC, Gutiérrez A, Rodríguez IM, Ibarra D, Martínez ÁT. Composition of non-woody plant lignins and cinnamic acids by Py-GC/MS, Py/TMAH and FT-IR. J Anal Appl Pyrolysis. 2007;79(1–2):39–46. doi:10.1016/j.jaap.2006.09.003.
32. Sokhansanj S. Baling biomass: densification and energy requirements. In: Holden NM, Wolfe ML, Ogejo JA, Cummins EJ, editors. Introduction to biosystems engineering. Virginia Tech Publishing; 2020.
33. Iqbal HMN, Asgher M, Bhatti HN. Optimization of physical and nutritional factors for synthesis of lignin degrading enzymes by a novel strain of Trametes vericolor. Bioresourses. 2011;6(2):1273–87. doi:10.15376/biores.6.2.1273-1287.
34. Janusz G, Pawlik A, Sulej J, Świderska-Burek U, Jarosz-Wilkołazka A, Paszczyński A. Lignin degradation: microorganisms, enzymes involved, genomes analysis and evolution. FEMS Microbiol Rev. 2017;41(6):941–62. doi:10.1093/femsre/fux049.
35. del Río JC, Rencoret J, Marques G, Li J, Gellerstedt G, Jimenez-Barbero J, et al. Structural characterization of the lignin from jute (*Corchorus capsularis*) fibers. J Agric Food Chem. 2009;57(21):10271–81. doi:10.1021/jf900815x.
36. Barbooti MM, Al-Sammerrai DA. Thermal decomposition of citric acid. Thermochimica Acta. 1986;98:119–26. doi:10.1016/0040-6031(86)87081-2.
37. Wyrzykowski D, Hebanowska E, Nowak-Wiczk G, Makowski M, Chmurzyński L. Thermal behaviour of citric acid and isomeric aconitic acids. J Therm Anal Calorim. 2010;104(2):731–5. doi:10.1007/s10973-010-1015-2.
38. Moldoveanu SC. Chapter 12-pyrolysis of carboxylic acids. In: Moldoveanu SC, editor. Pyrolysis of organic molecules. 2nd ed. Amsterdam, The Netherlands, Elsevier; 2019. p. 483–553.
39. Costigan S, Rawlinson C, Frosina J, McAdam K. Citric acid—A precursor to a respiratory sensitiser in e-cigarettes? In: Annual Meeting of the Society for Research on Nicotine and Tobacco; 2017; Florence, Italy.
40. Santoso M, Widyorini R, Prayitno TA, Sulistyo J. The effects of extractives substances for bonding performance of three natural binder on nipa fronds particleboard. KnE Life Sci. 2019;4(11):227–38. doi:10.18502/kls.v4i11.3868.
41. Mongiovi C, Lacalamita D, Morin-Crini N, Gabrion X, Ivanovska A, Sala F, et al. Use of chenevotte, a valuable co-product of industrial hemp fiber, as adsorbent for pollutant removal. Part I: chemical, microscopic, spectroscopic and thermogravimetric characterization of raw and modified samples. Molecules. 2021;26(15):4574. doi:10.3390/molecules26154574.

42. Moonart U, Utara S. Effect of surface treatments and filler loading on the properties of hemp fiber/natural rubber composites. Cellulose. 2019;26(12):7271–95. doi:10.1007/s10570-019-02611-w.
43. Liu Q, Niu S, Hu S, Cui X, Shi Z, Wu J, et al. Lignocellulose degradation pattern and structural change of the sawdust substrate and enzyme secretion by Lentinula edodes during its production. Wood Sci Technol. 2023;57:389–405. doi:10.1007/s00226-023-01460-y.
44. Diakité MS, Lenormand H, Lequart V, Arufe S, Martin P, Leblanc N. Cell wall composition of hemp shiv determined by physical and chemical approaches. Molecules. 2021;26(21):6334. doi:10.3390/molecules26216334.
45. Pandey KK. A study of chemical structure of soft and hardwood and wood polymers by FTIR spectroscopy. J Appl Polym Sci. 1999;71(12):1969–75. doi:10.1002/(ISSN)1097-4628.
46. Viel M, Collet F, Lanos C. Chemical and multi-physical characterization of agro-resources' by-product as a possible raw building material. Ind Crops Prod. 2018;120:214–37. doi:10.1016/j.indcrop.2018.04.025.
47. Gandolfi S, Ottolina G, Riva S, Fantoni GP, Patel I. Complete chemical analysis of carmagnola hemp hurds and structural features of its components. BioResources. 2013;8(2):2641–56. doi:10.15376/biores.8.2.2641-2656.
48. Fatriasari W, Syafii W, Wistara NJ, Syamsu K, Prasetya B. The characteristic changes of betung bamboo (*Dendrocalamus asper*) pretreated by fungal pretreatment. Int J Renew Energy Dev. 2014;3(2):11. doi:10.14710/ijred.3.2.133-143.
49. Sadrmanesh V, Chen Y. Bast fibres: structure, processing, properties, and applications. Int Mater Rev. 2018;64:1–26. doi:10.1080/09506608.2018.1501171.
50. Yang H, Yan R, Chen H, Lee DH, Zheng C. Characteristics of hemicellulose, cellulose and lignin pyrolysis. Fuel. 2007;86(12–13):1781–8. doi:10.1016/j.fuel.2006.12.013.
51. Lomelí-Ramírez MG, Kestur SG, Manríquez-González R, Iwakiri S, de Muniz GB, Flores-Sahagun TS. Bio-composites of cassava starch-green coconut fiber: part II–structure and properties. Carbohydr Polym. 2014;102:576–83. doi:10.1016/j.carbpol.2013.11.020.
52. Liu M, Fernando D, Daniel G, Madsen B, Meyer AS, Ale MT, et al. Effect of harvest time and field retting duration on the chemical composition, morphology and mechanical properties of hemp fibers. Ind Crops Prod. 2015;69:29–39. doi:10.1016/j.indcrop.2015.02.010.

Appendix A

Methods: Thermo-Chemical Equipment

Pyrolysis-Gas Chromatography-Mass Spectrometry (Py-GC/MS)

Py-GC/MS was utilized to screen and compare the chemical composition of the raw hemp hurd. About 500 µg per sample were placed in an eco-cup SF PY1-EC50F, covered with glass wool, and pyrolyzed at 500°C for 0.1 min using a multi-shot pyrolyzer (EGA/PY-3030D). The pyrolyzer was connected (interface temperature: 280°C) to a GC/MS system QP-2020 NX (Shimadzu, Japan) with an SH-Rxi-5Sil MS column (30 m × 0.25 mm, 0.25 µm film thickness) at 20.0 kPa pressure (15.9 mL/min, 0.61 mL/min column flow) using helium as a carrier gas, and 70 eV electron impact. The GC temperature profile involved a 1-min hold at 50°C, followed by a temperature increase to 280°C (5°C/min) and a 13-min hold at 280°C. Identification of pyrolysis products relied on comparing their retention times and mass spectra data with NIST LIBRARY 2017.14 (35).

Fourier-Transform Infrared Spectroscopy (FTIR)

FTIR was used to investigate potential structural differences among various raw hemp hurd samples. The analysis employed a Spectrum two instrument (Perkin Elmer Inc., Waltham, MA, USA) with Attenuated Total Reflection (ATR) mode, equipped with Spectrum software (Ver. 10.5.3, Perkin Elmer Inc., USA). Spectra were recorded from approximately 0.1 g of the sample placed on a diamond plate, involving 16 scans in absorption mode at a 4.0 cm^{-1} resolution, covering wavelengths ranging from 4000 to 400 cm^{-1}.

Thermogravimetric Analysis (TGA)

TGA was used to compare the thermal stability characteristics of hemp hurd from different cultivars with varying harvesting times and retting durations. Samples weighing about 10 mg ± 0.1 mg were placed in the crucible pan of a Thermogravimetric Analyzer (TGA 4000, Perkin Elmer Inc., USA) and subjected to heating at a rate of 10°C/min from 25°C to 500°C. To prevent oxidation, a flow of nitrogen gas at 20 mL/min was maintained during the analysis. Pyris software (Ver. 11.1.1, Perkin Elmer Inc., USA) was employed to calculate the weight loss (TG) and differential thermogravimetry (DTG) for each sample.